Title: Beclin-1-mediated activation of autophagy improves proximal and distal urea cycle disorders.

Authors: Leandro R. Soria (*a*), Dany P. Perocheau (*b*), Giulia De Sabbata (*c*), Angela De Angelis (*a*), Gemma Bruno (*a*), Elena Polishchuk (*a*), Sonam Gurung (*b*), Debora Paris (*d*), Paola Cuomo (*d*), Andrea Motta (*d*), Michael Orford (*b*), Simon Eaton (*b*), Simon Waddington (*b, e*), Carmine Settembre (*a*), Andrés F. Muro (*c*), Julien Baruteau *(b, f)*, and Nicola Brunetti-Pierri (*a, g*).

Institutions: ***(a)*** Telethon Institute of Genetics and Medicine, Pozzuoli, Italy; ***(b)*** UCL Great Ormond Street Institute of Child Health, London, UK; ***(c)*** International Centre for Genetic Engineering and Biotechnology, Trieste, Italy; ***(d)*** Institute of Biomolecular Chemistry, National Research Council, Pozzuoli, Italy; ***(e)*** Wits/SAMRC Antiviral Gene Therapy Research Unit, Faculty of Health Sciences, University of the Witwatersrand, Johannesburg, South Africa; ***(f)*** Metabolic Medicine Department, Great Ormond Street Hospital for Children NHS Foundation Trust, London, UK; ***(g)*** Department of Translational Medicine, Federico II University, Naples, Italy.

Corresponding author: Nicola Brunetti-Pierri, M.D.

Telethon Institute of Genetics and Medicine

Via Campi Flegrei 34

Phone: +39 081 19230661

Fax: +39 081 5609877

E-mail: brunetti@tigem.it

Running title: Beclin-1 for urea cycle disorder therapy

Keywords: urea cycle disorders/ OTC deficiency/ argininosuccinic aciduria/ autophagy/ Tat-Beclin-1 peptide.

ABSTRACT

Urea cycle disorders (UCD) are inherited defects in clearance of waste nitrogen with high morbidity and mortality. Novel and more effective therapies for UCD are needed. Studies in mice with constitutive activation of autophagy unraveled Beclin-1 as *druggable* candidate for therapy of hyperammonemia. Next, we investigated efficacy of cell penetrating autophagy inducing Tat-Beclin-1 (TB-1) peptide for therapy of the two most common UCD, namely ornithine transcarbamylase (OTC) and argininosuccinate lyase (ASL) deficiencies. TB-1 reduced urinary orotic acid and hyperammonemia, and improved survival under protein-rich diet in *spf-ash* mice, a model of OTC deficiency (proximal UCD). In $Asl^{Neo/Neo}$ mice, a model of ASL deficiency (distal UCD), TB-1 increased ureagenesis, reduced argininosuccinate, and improved survival. Moreover, it alleviated hepatocellular injury and decreased both cytoplasmic and nuclear glycogen accumulation in $Asl^{Neo/Neo}$ mice. In conclusion, Beclin-1-dependent activation of autophagy improved biochemical and clinical phenotypes of proximal and distal defects of the urea cycle.

INTRODUCTION

Autophagy is highly active in liver. Proteins, glycogen, and lipid droplets are degraded by autophagy in liver cells to release amino acids, glucose, and free fatty acids that can be reused for synthesis of new proteins and macromolecules, or can enter the tricarboxylic acid (TCA) cycle to generate ATP (Kaur & Debnath, 2015). Liver autophagy was recently found to support ammonia detoxification by furnishing the urea cycle with intermediates and energy that increase urea cycle flux under conditions of excessive ammonia (Soria et al, 2018). Liver-specific deficiency of autophagy impaired ammonia detoxification whereas its enhancement resulted in increased urea synthesis and protection against hyperammonemia (Soria et al, 2018). Therefore, drugs enhancing autophagy have potential for treatment of urea cycle disorders (Soria & Brunetti-Pierri, 2018; Soria & Brunetti-Pierri, 2019). In a previous study (Soria et al, 2018), we showed that rapamycin reduces orotic acid in *spf-ash* mice, a mouse model of the ornithine transcarbamylase (OTC) deficiency that carries a single nucleotide mutation in the fourth exon of the *Otc* gene resulting in a splicing defect and 10% of residual enzyme activity (Hodges & Rosenberg, 1989). Although it has been efficiently used to promote autophagy, rapamycin does not completely inhibit its target, the mechanistic target of rapamycin kinase complex 1 (mTORC1) and affects several biological processes besides autophagy (Li et al, 2014). Therefore, drugs targeting autophagy more specifically are more attractive because they are expected to have less side effects. Tat-Beclin-1 (TB-1) is an engineered cell-permeable peptide that potently and specifically induces autophagy (Shoji-Kawata et al, 2013). TB-1 is formed by the HIV-1 Tat protein transduction domain attached via a diglycine linker to a peptide derived from Beclin-1 (*Becn1*), a key component of the autophagy induction machinery (Shoji-Kawata et al, 2013). In summary, TB-1 is an attractive therapeutic candidate for its specificity and safety at least in mice, and has shown great potential for treatment of various diseases, including several types of cancer, infections, cardiac dysfunction, skeletal disorders, and

axonal injuries (Bartolomeo et al, 2017; Cinque et al, 2015; He et al, 2016; Pietrocola et al, 2016; Song et al, 2018; Sun et al, 2018; Vega-Rubin-de-Celis et al, 2018). In the present study, we investigated the therapeutic potential of TB-1 for treatment of urea cycle disorders (UCD).

RESULTS

Constitutional hyperactivation of Beclin-1 enhances ammonia detoxification.

Beclin-1 is a central player in autophagy and regulates autophagosome formation and maturation (Liang et al, 2008). To investigate *Becn1* functions *in vivo*, a knock-in mouse model carrying a *Becn1* mutation (*Becn1*^{F121A}) resulting in constitutively active autophagy has been recently generated (Rocchi et al, 2017). In these mice Phe121 is mutated into alanine resulting in disruption of the BECN1-BCL2 binding and constitutive activation of BECN1 and autophagy in multiple tissues, including liver (Fernandez et al, 2018; Rocchi et al, 2017; Yamamoto et al, 2018). In these mice, we investigated ammonia detoxification by measurements of blood ammonia levels during acute hyperammonemia induced by an ammonia challenge. Despite no changes in blood ammonia at baseline, *Becn1*^{F121A} mice showed 32% reduction in blood ammonia at 30 min after intra-peritoneal (i.p.) injection of ammonium chloride compared to age-matched wild-type (WT) mice (**Fig. 1A**). Accordingly, *Becn1*^{F121A} mice showed enhanced ureagenesis compared to WT controls, as shown by increased blood levels of ^{15}N-labeled urea from ^{15}N-ammonium chloride (**Supp. Fig. 1A**). Improved ammonia clearance was not dependent on increased expression of urea cycle enzymes in *Becn1*^{F121A} mice that showed similar enzyme levels by Western blotting compared to WT controls (**Supp. Fig. 1B** and **C**). Therefore, consistent with previous findings (Soria et al, 2018), gain-of-function mutation of the autophagy activator *Becn1* protects against acute hyperammonemia *in vivo*, suggesting that Beclin-1 is a *druggable* candidate for therapy of hyperammonemia.

Tat-Beclin-1 improves the phenotype of OTC deficient mice.

To investigate the therapeutic efficacy of *Becn1*-mediated induction of autophagy in mouse models of UCD, we injected TB-1 i.p. in *spf-ash* mice (Hodges & Rosenberg, 1989), a model of OTC deficiency, the most common UCD. Although not normalized, in *spf-ash* mice the levels of the biochemical hallmark of OTC deficiency, urinary orotic acid, were significantly reduced by TB-1 (**Fig. 1B**). Consistent with its autophagy enhancer activity, TB-1 increased the hepatic autophagic flux, as showed by reduced protein levels of the autophagosome marker LC3-II, and the two main autophagy cargo receptors, namely p62 and NBR1 (**Fig. 1C** and **D**). Notably, OTC residual enzyme activity was unaffected by TB-1 (**Supp. Fig. 2**), thus excluding reduction of urinary orotic acid as a consequence of increased residual OTC activity induced by TB-1. To further investigate the efficacy of TB-1-mediated increased liver autophagy for therapy of OTC deficiency, *spf-ash* mice were fed for ten days with a high protein diet and were either treated with TB-1 or left untreated. Consistent with previous reports (Kurtz et al, 2019; Yang et al, 2016), *spf-ash* mice showed marked mortality under high protein diet compared to control WT mice (**Fig. 1E**). Although it did not significantly improved survival as single treatment, when combined with an ammonia scavenger drug (Na-benzoate) and L-arginine (L-Arg), TB-1 increased survival whereas ammonia scavengers and L-Arg did not affect survival of *spf-ash* mice under high protein diet (**Fig. 1E**). Consistent with the increased survival, blood ammonia levels measured after four days with high protein diet (a time-point prior to mortality) were significantly lower in *spf-ash* mice treated with the combination of TB-1 and Na-benzoate and L-Arg compared to untreated *spf-ash* mice (**Fig. 1F**). TB-1 alone decreased slightly but not significantly blood ammonia whereas Na-benzoate and L-Arg significantly reduced blood ammonia levels, consistent with previous data (Enns et al, 2007) (**Fig. 1F**). Taken together, these results support the therapeutic potential of activation of liver autophagy

by TB-1 in combination with conventional treatments, such as ammonia scavenger drugs and L-Arg (Enns et al, 2007; Haberle et al, 2019), for treatment of OTC deficiency, the most common UCD (DeMars et al, 1976).

Tat-Beclin-1 enhances ureagenesis and corrects metabolic abnormalities of argininosuccinic aciduria.

To investigate the efficacy of autophagy enhancement for therapy of argininosuccinic aciduria (ASA), the second most frequent UCD(Baruteau et al, 2019a), we investigated TB-1 treatment in the hypomorphic murine model of ASL deficiency ($Asl^{Neo/Neo}$) that expresses approximately 16% of residual enzyme activity and recapitulates the main biochemical and clinical abnormalities of ASA patients (Baruteau et al, 2018; Burrage et al, 2020; Kho et al, 2018; Nagamani et al, 2012). Besides impaired urea synthesis and ammonia detoxification, systemic manifestations of ASA, such as reduced body weight, increased blood pressure, and reduced survival are also associated with nitric oxide (NO)-deficiency (Baruteau et al, 2018; Erez et al, 2011; Kho et al, 2018; Nagamani et al, 2012). $Asl^{Neo/Neo}$ mice treated only with TB-1 showed increased survival compared to vehicle-treated controls that started dying by ten days of age (**Fig. 2A**). Consistent with our previous work (Soria et al, 2018), TB-1-mediated activation of autophagy in $Asl^{Neo/Neo}$ mice was associated with increased incorporation of ^{15}N into urea (+88%, $p<0.05$) indicating enhanced ureagenesis (**Fig. 2B**). As expected, autophagic flux was enhanced in livers of $Asl^{Neo/Neo}$ mice injected with TB-1, as shown by reduced LC3-II and decreased autophagy substrates (p62 and NBR1) in livers (**Fig. 2C** and **D**), whereas residual ASL enzyme activity was unaffected (**Supp. Fig. 3**). Metabolomic analysis by ^{1}H-NMR spectroscopy (Soria et al, 2018) showed that the whole-liver metabolome of vehicle-treated $Asl^{Neo/Neo}$ mice was well separated from healthy WT controls but it was shifted towards non-diseased WT controls in $Asl^{Neo/Neo}$ mice injected with TB-1

(**Fig. 2E**), suggesting that TB-1 corrects at least partially the liver metabolic deregulation caused by ASL deficiency. Consistent with this finding, argininosuccinic acid was reduced in livers (**Fig. 2F**) and dried blood spots in TB-1-treated *Asl*$^{Neo/Neo}$ mice (**Supp. Fig. 4**). Notably, liver contents of the two precursors of argininosuccinate, namely citrulline and aspartate, were also normalized (**Supp. Fig. 5**). Moreover, levels of key compounds of the TCA cycle (fumarate and succinate) and glucose were rescued by TB-1 (**Supp. Fig. 5**). In summary, TB-1 improved several biochemical alterations of ASA, confirming the efficacy of autophagy enhancer molecules for therapy of UCD.

Tat-Beclin-1 reduced injury and abnormal glycogen deposition in livers with ASL deficiency.

Chronic hepatocellular injury is a common complication in patients with ASL deficiency (Baruteau et al, 2017; Mori et al, 2002; Ranucci et al, 2019; Yaplito-Lee et al, 2013). Despite the underlying mechanism triggering the liver disease remains unclear, evidence in human and mouse suggests that it is related to massive accumulation of cytoplasmic glycogen (Badizadegan & Perez-Atayde, 1997; Bigot et al, 2017; Burrage et al, 2020). Moreover, because activation of autophagy was found to be effective in clearance of glycogen storage in glycogen storage diseases (Ashe et al, 2010; Farah et al, 2016; Martina et al, 2014; Spampanato et al, 2013), we investigated whether TB-1 promotes glycogen clearance in ASA livers. To this end, *Asl*$^{Neo/Neo}$ mice received protein-restricted diet and daily administration of Na-benzoate and L-Arg in combination with either TB-1 or vehicle, started on day ten of life and lasting for 3 weeks. Consistent with previous data (Ashley et al, 2018; Baruteau et al, 2018; Burrage et al, 2020; Erez et al, 2011), vehicle-treated *Asl*$^{Neo/Neo}$ mice showed vacuolated hepatocyte cytoplasm by hematoxylin and eosin (H&E) staining in contrast to WT mice, whereas TB-1 treatment markedly improved the microscopic changes of liver architecture (**Fig. 3A**). Moreover, *Asl*$^{Neo/Neo}$ mice treated with TB-1 showed marked reduction of liver glycogen storage by periodic acid Schiff (PAS) staining (**Fig. 3A** and **B**) and glycogen quantification (**Fig.**

3C) compared to controls. Notably, glycogen accumulation was not observed in livers of *spf-ash* mice (**Supp. Fig. 6**). Glycogen in hepatocytes is catabolized either in cytosol by the coordinated action of enzymes involved in glycogenolysis or in the lysosome by the acid glucosidase (Prats et al, 2018). Hepatic expression of glycogen phosphorylase (PYGL), the enzyme that catalyzes the rate limiting step of glycogenolysis, was recently found to be reduced in $Asl^{Neo/Neo}$ mice, suggesting a mechanism responsible for aberrant glycogen accumulation in ASA (Burrage et al, 2020). We confirmed reduced PYGL protein levels in livers of $Asl^{Neo/Neo}$ mice, but they were unaffected by TB-1 (**Fig. 3D**), suggesting that reduction of glycogen by TB-1 does not occur through rescue of the cytosolic glycogen degradation pathway. Moreover, when autophagy flux is increased by TB-1, glycogen degradation in lysosomes is efficiently achieved, as confirmed by electron microscopy (EM) analysis showing clearance of cytoplasmic glycogen accumulation (**Fig. 3E**). Moreover, glycogen accumulation in $Asl^{Neo/Neo}$ mice resulted in displacement of organelles to the cell membrane as previously reported (Burrage et al, 2020), that is relieved by TB-1 (**Fig. 3E**). Surprisingly, EM analysis also showed abundant intra-nuclear glycogen deposition in hepatocytes of $Asl^{Neo/Neo}$ mice, that was markedly reduced by TB-1 (**Fig. 4A** and **B**). In summary, in addition to promoting urea synthesis, TB-1 reduced abnormal glycogen storage in cytosol and nuclei of ASL-deficient hepatocytes.

DISCUSSION

UCD are inborn errors of metabolism due to impaired clearance of toxic nitrogen. Despite current therapies, cumulative morbidity is still high in patients with UCD and thus, several experimental therapies have been investigated to improve clinical outcomes (Soria et al, 2019). We recently showed a role of hepatic autophagy in promoting ureagenesis and ammonia detoxification (Soria et al, 2018) that can be exploited for the development of novel therapies for

hyperammonemia and UCD (Soria et al, 2018; Soria & Brunetti-Pierri, 2018; Soria & Brunetti-Pierri, 2019). In the present study, we investigated the efficacy of TB-1 peptide, a potent and specific agent that can activate autophagy *in vivo*, in two well-established mouse models of proximal and distal UCD. Induction of liver autophagy was found to improve several clinically relevant endpoints in these mice, supporting autophagy enhancement as a therapeutic strategy for UCD.

Autophagy plays a key role in liver physiology by supporting metabolism and promoting adaptation to stress. Specific modulation of autophagy has been recognized as a potential therapeutic strategy in various liver diseases (Allaire et al, 2019; Hazari et al, 2020). Obtaining specific modulation of autophagy has been a major challenge for clinical translation of autophagy enhancer molecules (Allaire et al, 2019). Being an essential regulator of autophagosome synthesis and maturation, Beclin-1 is an attractive target for autophagy-inducing drugs and small peptides affecting Beclin-1 interactions, such as TB-1 and its derivatives have been developed (Peraro et al, 2017; Shoji-Kawata et al, 2013). Moreover, drugs affecting post-translational modifications of Beclin-1 altering its function are also attractive (Hill et al, 2019). The *Becn1*^{F121A} mouse model used in this work mimics the condition of disrupted interaction of Beclin-1 with BCL2. In these mice, we found improved ureagenesis and increased ammonia detoxification capacity. Within the context of a normal functioning ureagenesis, the increase detected in *Becn1*^{F121A} mice was relatively mild and corresponded to about 20-30%. Nevertheless, such increase is still expected to provide significant clinical benefit in UCD. Additionally, the increased ureagenesis of *Becn1*^{F121A} mice validates the inhibitors of the Beclin-1-BCL2 complex (Chiang et al, 2018) as targets for increasing ammonia detoxification.

We next investigated the efficacy of TB-1-mediated activation of hepatic autophagy for therapy of proximal and distal UCD using the most relevant mouse models for these disorders, the

spf-ash and the *Asl*$^{Neo/Neo}$ mice for OTC- and ASL-deficiencies, respectively (Kurtz et al, 2019; Moscioni et al, 2006; Prieve et al, 2018; Soria et al, 2019). In *spf-ash* mice treated with TB-1, we detected reduced urinary orotic aciduria and hyperammonemia under standard and high protein diet, respectively. Importantly, combined with clinically available drugs enhancing ammonia excretion (Na-Benzoate) and urea synthesis (L-Arg), TB-1 was also effective in increasing survival of *spf-ash* mice challenged with a high protein diet. These data suggest that liver autophagy enhancement cooperates with current treatment in improving the phenotype of OTC deficiency. In ASA mice, we also found that hepatic enhancement of autophagy increased ureagenesis and survival, and reduced argininosuccinate levels along with generalized rescue of the metabolic derangement, as suggested by liver metabolomic analyses. In summary, TB-1 improved the phenotypes of two UCD animal models, supporting the potential of autophagy enhancement for therapy of hyperammonemia due to defects of the urea cycle.

Interestingly, in ASA mice TB-1 also resulted in increased clearance of intracellular glycogen accumulation. Disposal of carbohydrates such as glycogen via autophagy plays a crucial role in glucose homeostasis (Karsli-Uzunbas et al, 2014). This finding is consistent with previous studies in glycogen storage diseases type 1 and 2 showing that either genetic or pharmacologic activation of autophagy reduced glycogen storage (Ashe et al, 2010; Farah et al, 2016; Martina et al, 2014; Spampanato et al, 2013). Consistent with a previous study (Burrage et al, 2020), we found that PYGL was reduced in ASL-deficient mice and thus, increased glycogen degradation mediated by TB-1 occurred independently from impaired cytosolic PYGL-dependent degradation of glycogen.

Glycogen clearance induced by TB-1 restored physiologic organelle distribution within the cell. Abnormal glycogen deposition in UCD livers occurs independently from metabolic syndrome (Bigot et al, 2017) and has been reported in patients with OTC deficiency and other UCD

(Badizadegan & Perez-Atayde, 1997; Baruteau et al, 2017; Bigot et al, 2017; Mori et al, 2002; Ranucci et al, 2019; Yaplito-Lee et al, 2013). However, *spf-ash* mice showed normal hepatic glycogen storage. Intriguingly, we found glycogen accumulation also in nuclei of ASA hepatocytes. Nuclear accumulation of glycogen was recently associated to epigenetic changes in gene expression and cancer (Sun et al, 2019). Moreover, liver cancer is an emerging feature of UCD (Koo et al, 2017; Wang et al, 2019; Wilson et al, 2012). Therefore, besides improved ureagenesis, the reduced cytoplasmic and intranuclear glycogen mediated by TB-1 might provide further long-term clinical benefits preventing progression of chronic liver damage. However, this hypothesis would need further investigation and available mouse models of UCD have not been reported to have an increased frequency of liver cancer. The newly generated OTC knock-out mouse model that develops liver fibrosis and chronic liver damage (Wang et al, 2017) might be a suitable model to investigate this issue in long-term studies.

In conclusion, this study shows a key role of liver autophagy in nitrogen homeostasis and indicates that Beclin-1 as a *druggable* target for therapy of hyperammonemia and UCD. Moreover, these findings show that enhancement of hepatic autophagy is beneficial in UCD through: *i)* correction of the underlying metabolic abnormalities by supporting residual ureagenesis activity and, *ii)* reduction of the aberrant intracellular (cytosolic and nuclear) glycogen burden that may prevent long-term hepatotoxicity.

MATERIALS AND METHODS

Mouse studies. All mouse procedures were performed in accordance with regulations and were authorized by either the Italian Ministry of Health or the UK Home Office. *Becn1*^{F121A} mice were previously described (Fernandez et al, 2018; Rocchi et al, 2017) and were maintained on a C57BL/6 background. Wild-type (WT) littermates were used as controls. For acute ammonia challenges,

male and female WT and *Becn1*^{F121A} mice were starved overnight before the intraperitoneal (i.p.) injection of 10mmol/kg of ^{15}N-labeled ammonium chloride (98% enriched in ^{15}N, Sigma) dissolved in water. Blood samples were collected by retro-orbital bleedings at baseline, 5, 15, and 30 min post-injection. The amount of ^{15}N-labeled urea in sera was quantified by gas chromatography–mass spectrometry (GC-MS) analysis at the Metabolic Core of The Children's Hospital of Philadelphia (Philadelphia, PA). Mice were sacrificed by cervical dislocation, and liver samples were harvested for analyses. Breeding pairs of *spf-ash* mice (B6EiC3Sn a/A-OTC$^{Spf\text{-}Ash}$/J) were purchased from Jackson Laboratories (Cat# 001811) and housed in individually ventilated cages, maintaining a temperature of 22°C (± 2°C), relative humidity of 55% (± 10%), 15-20 air exchanges per hour and 12-h light/12-h dark cycle and receiving a standard chow diet and water *ad libitum*. 12 week-old male *spf-ash* mice received an i.p. injection of TB-1 D-11 retroinverso form peptide (Novus Biologicals; Cat# NBP2-49888) at the dose of 15 mg/kg [dissolved in phosphate buffer saline (PBS)] every 48 h for a total period of 10 days. Animals were daily monitored and weighted. Urine samples were collected at the indicated time points to measure orotic acid. A control group of *spf-ash* animals were injected with vehicle only. For high protein diet challenge, 12 weeks old male *spf-ash* mice were maintained on a 51%-protein diet (U8959 version 142, Safe-diets) for 10 days. TB-1 peptide was delivered by i.p. injection at the dose of 15 mg/kg every 48 h. Ammonia scavenger solution, consisting of 60 mg/ml Na-Benzoate (Sigma; Cat# 18106) and 60 mg/ml L-Arg (Sigma, Cat# A5006) dissolved in PBS, was i.p. injected at the dose of 250 mg/kg Na-Benzoate, 250 mg/ml L-Arg every 24 h. As controls, a group of *spf-ash* mice were injected with vehicle only and a group of WT mice were used. Animals were daily monitored and weighted. Blood samples were collected by submandibular bleeding at day 4 to measure ammonia concentration.

Asl$^{Neo/Neo}$ mice (B6.129S7-*Asl*^{tm1Brle}/J) were purchased from Jackson Laboratory (Bar Harbor, ME) and maintained on standard rodent chow (Harlan 2018, Teklab Diets, Madison, WI;

protein content 18%) with free access to water in a 12 h light/12 h dark environment. For mouse genotyping, DNA extraction from tail clips was performed as described previously (Baruteau et al, 2018). For long-term experiment, all WT and *Asl*$^{Neo/Neo}$ mice received a supportive treatment modified (Baruteau et al, 2018) including a reduced-protein diet (5CR4, Labdiet, St Louis, MO; protein content 14.1%) and daily i.p. injections of Na-benzoate (0.5g/kg/d) and L-Arg (0.5g/kg/d) from day 10 to day 30. Treated *Asl*$^{Neo/Neo}$ mice received 15mg/kg of TB-1 i.p. three times per week (Monday, Wednesday, Friday). Control animals received vehicle (*i.e.* PBS). Male WT and *Asl*$^{Neo/Neo}$ mice received three i.p. injections over 5 or 20 days with either PBS or TB-1 from 10 days-old onwards. Concomitantly, these mice received daily supportive treatment to improve survival until day 30. WT littermates were used as controls. For all experiments, WT and *Asl*$^{Neo/Neo}$ littermates were housed in the same cages.

Biochemical measurements. Blood ammonia levels were measured by ammonia colorimetric assay kits (BioVision Incorporated; Cat# K370-100 or Sigma; Cat#AA0100) according to the manufacturer's instructions. Orotic acid was purchased from Sigma-Aldrich. The isotopically labeled internal standard orotic acid was purchased from Cambridge Isotope Laboratories, Inc. The quantitative experiments were done using as internal standard the isotopically labeled 1,3-$^{15}N_2$ orotic acid in 200µM concentration both for calibration curve and samples. A typical calibration curve ranged from 15µM to 300µM with excellent linearity (R^2>0.99). A Bruker (Bremen, Germany) amaZon SL bench-top ion trap mass spectrometer, equipped with an electrospray source, was employed for this study. The source was operated in negative ion mode with a needle potential of 4500V and a gas flow of 12L/min of nitrogen with heating at 200°C. The chromatographic separations for quantitative experiments were performed using a series 1260 Agilent Technologies (Waldbronn, Germany) HPLC with auto sampler controlled from the Bruker Hystardata system. A

Phenomenex (Torrance, USA) HPLC column Gemini C18 5µm, 110Å, 2x150mm was employed. Column flow rate was 0.4 mL/min and elution was performed using 5min wash time after 10µl injection and a 3 min gradient from water with 0.1% formic acid to 90% acetonitrile with 0.1% formic acid. The tandem mass spectrometry (MS/MS) transitions used for the quantitative experiments (multiple reaction monitoring, MRM) were m/z 155.1 to 111.1 (orotic acid) and 157.1 to 113.1 (1,3-15N2 orotic acid). The acquired data were processed using the Bruker Compass Data Analysis proprietary software. Creatinine was measured using the Mouse Creatinine kit (Crystal Chem; Cat# 80350) following the manufacturer's guidelines and used to normalize orotic acid values in the urine.

Mass spectrometry analysis of argininosuccinic acid in dried bloodspots was performed as previously described (Baruteau et al, 2019b). Briefly, blood spots on a Guthrie card were dried at room temperature for 24 h. 3mm-diameter punch from dried blood spots were used to measure argininosuccinic acid by liquid chromatography-tandem mass spectrometry (LC-MS/MS). A punch was incubated for 15 min in sonicating water bath in 100 µL of methanol containing stable isotopes used as internal standards. A 4:1 volume of methanol was added to precipitate contaminating proteins. The supernatant was collected and centrifuged at 16,000 g for 5 min before separation on a Waters Alliance 2795 LC system (Waters, Midford, USA) using a XTerra® RP18, 5 µm, 3.9 x 150mm column (Waters, Midford, USA). The mobile phases were (A) methanol (B) 3.7% acetic acid. Detection was performed using a tandem mass spectrometer Micro Quattro instrument (Micromass UK Ltd, Cheshire, UK) using multiple reaction monitoring in positive ion mode. Data were analysed using Masslynx 4.1 software (Micromass UK Ltd, Cheshire, UK).

***In vivo ^{15}N-ureagenesis in Asl$^{Neo/Neo}$* mice.** Vehicle- and TB-1-treated *Asl$^{Neo/Neo}$* mice received an i.p. injection of 4 mmol/kg of ^{15}N-labeled ammonium chloride ($^{15}NH_4Cl$, Cambridge Isotope

Laboratories) 20 min before terminal blood collection via cardiac puncture. Blood was collected in 1:10 volume of sodium citrate and centrifuged at 13,000 g for 5 min. Plasma was collected and snap frozen in dry ice. $^{13}C,^{15}N_2$-urea (Sigma) was added to all samples as an internal standard, and samples were derivatized in a two-stage procedure. Firstly, urea was cyclized with 1,1,3,3-Tetramethoxypropane (Sigma-Aldrich) under acidic conditions to obtain 2-hydroxypyrimidine (2HP). 2HP was then coupled with 2,3,4,5,6-Pentafluorobenzyl bromide (Sigma-Aldrich) to yield a derivative that, upon negative ion chemical ionization gas-chromatography mass spectrometry, yields a negatively charged 2-HP fragment that includes the nitrogen and carbon atoms of the starting urea. Ions of mass/charge 95 (2HP from $^{12}C,^{14}N_2$-urea), 96 ($^{12}C,^{15}N,^{14}N$-urea derived from ^{15}N-ammonium chloride or $^{13}C,^{14}N_2$-urea) and 98 ($^{13}C,^{15}N_2$-urea internal standard) were analyzed, and quantified with suitable standard curves (95/98 for unlabeled urea, 96/98 for ^{15}N-urea). Unlabelled urea concentration was calculated from the 95/98 ratio, the contribution of unlabelled urea to mass 96 calculated from the natural abundances of the atoms in the fragment ($C_4H_3N_2O^-$), and ^{15}N-urea calculated from the 96/98 ratio minus the contribution of unlabelled urea to mass 96.

Metabolite profiling of liver tissue by ^{1}H-NMR. Livers were mechanically disrupted to extract the metabolites of interest (lipids, carbohydrates, amino acids, and other low-molecular weight metabolites) while leaving other compounds (DNA, RNA, and proteins) in the tissue pellet. Homogenization of 200 mg of frozen tissue samples was carried out in cold methanol (8 ml per g of tissue, wet weight), and cold water (1.7 ml per g of tissue, wet weight) with UltraTurrax for 2 min on ice. Four ml of chloroform per g of tissue (wet weight) were added and the homogenate was gently stirred and mixed on ice for 10 min (the solution must be mono-phasic). Then, additional 4 ml of chloroform per g of tissue (wet weight), and 4 ml of water per g of tissue (wet weight) were

added and the final mixture was well shaken and centrifuged at 12,000 g for 15 min at 4°C. This procedure separates three phases: water/methanol on the top (aqueous phase with the polar metabolites), denatured proteins and cellular debris in the middle, and chloroform at the bottom (lipid phase with lipophilic compounds). The upper and the lower layers were transferred into glass vials, the solvents removed under a stream of dry nitrogen, and stored at -80°C until analysis. Polar extracts were re-suspended in 700 µl PBS, pH 7.4 with 10% D_2O for lock procedure, and then transferred into an NMR tube. High-resolution one-dimensional (1D) spectra were recorded at 600.13 MHz on a Bruker Avance III-600 spectrometer (Bruker BioSpin GmbH, Rheinstetten, Germany) equipped with a TCI CryoProbe^{TM} fitted with a gradient along the Z-axis, at a probe temperature of 27°C, using the excitation sculpting sequence for solvent suppression. Spectra were referenced to internal 0.1 mM sodium trimethylsilylpropionate (TSP), assumed to resonate at δ = 0.00 ppm.

NMR data processing and statistical analysis. The spectral 0.50–9.40 ppm region of the ^{1}H-NMR spectra was automatically data reduced to integrated regions (buckets) of 0.04-ppm each using the AMIX 3.6 package (Bruker Biospin GmbH, Rheinstetten, Germany). The residual water resonance region (4.72–5.10 ppm) was excluded, and the integrated region was normalized to the total spectrum area. To differentiate liver tissues through NMR spectra, we carried out a multivariate statistical data analysis using projection methods as previously reported[2].

Enzyme activity assays. OTC enzyme activity was determined in total liver protein extracts as reported previously(Ye et al, 1996) with minor modifications. One µg of total liver protein extract (in lysis buffer: 0.5% Triton-X, 10mM Hepes pH 7.4, 2mM DTT) was added to 350µl of reaction mixture (5mM ornithine, 15mM carbamyl phosphate and 270mM triethanolamine, pH 7.7) and

incubated at 37°C for 30min. The reaction was then stopped by adding 125 µl of 3:1 phosphoric/sulfuric acid solution followed by 25 µl of 3% 2,3-butanedione monoxime and incubated at 95°C for 15min in the dark. Citrulline production was determined by measuring the absorbance at 490nm. The assays were performed in duplicate.

Liver samples were snap-frozen in dry ice at time of collection. Protein extraction was performed on ice. Liver samples were homogenised with the Qiagen Bead Tissue Lyser (Qiagen Manchester Ltd, Manchester, UK) in 500µL of 50mM phosphate buffer (pH 7.4) with EDTA-free proteinase inhibitor cocktail (Roche, Basel, Switzerland) at a frequency of 30 for 30 sec. Homogenates were centrifuged at 13,000 g for 10 min at 4°C. Protein quantification of the supernatant was performed using the Pierce™ BCA protein assay kit (Thermo-Fisher Scientific, Rockford, IL, USA) according to the manufacturer's instructions. ASL activity was measured by synthesis of fumarate in an excess of argininosuccinate as previously described (Baruteau et al, 2018). Fumarate was measured with the Fumarate Assay Kit (Sigma; Cat# MAK060) according to manufacturer's instructions.

Periodic acid Schiff (PAS) staining. The staining was performed according to the Standard Operating Procedure protocol at the Histopathology laboratory, Great Ormond Street Hospital, London. Sections were dewaxed in xylene, hydrated down through graded alcohol solutions to water, incubated for 10 min in 0.5% periodic acid, rinsed in distilled water, stained for 10 min with Schiff reagent, then rinsed in distilled water. Sections were then washed for 5 min in running tap water and counterstained in 1% eosin for 1 min, rinsed briefly in running tap water and dehydrated through ascending grades of alcohol. Sections were then cleared in xylene and mounted. For hematoxylin and eosin (H&E) staining, liver sections were processed according to standard protocols.

For quantitative PAS staining quantification, ten random images per liver section were captured with a microscope camera (DFC420; Leica Microsystems, Milton Keynes, UK) and software (Image Analysis; Leica Microsystems). Quantitative analysis was performed with thresholding analysis using the Image-Pro Premier 9.1 software (Rockville, MD, USA).

Hepatic glycogen determination. Liver content of glycogen was determined by using a colorimetric glycogen assay kit (Sigma-Aldrich; Cat# MAK016). Liver lysates were made by homogenization following the manufacturer's instructions using a Tissue Lyser (Qiagen). Hepatic glycogen levels were normalized for protein concentrations determined by Bradford Reagent (Bio-Rad).

Western blotting. Liver specimens were homogenized in RIPA buffer in the presence of complete protease inhibitor cocktail (Sigma), incubated for 20 min at 4°C and centrifuged at 13,200 rpm for 10 min. Pellets were discarded and cell lysates were used for western blots. Total protein concentration in cellular extracts was measured using the Bradford Reagent (Bio-Rad). Protein extracts were separated by SDS–PAGE and transferred onto polyvinylidene difluoride (PVDF) membranes. Blots were blocked with TBS-Tween-20 containing 5% non-fat milk for 1 h at room temperature followed by incubation with primary antibody overnight at 4°C. The primary antibodies used were: rabbit anti-LC3B (Novus Biologicals; Cat# NB-100-2220), mouse anti-p62 (Abnova; Cat# H00008878-M01), mouse anti-NRB1 (Abnova; Cat# H00004077-M01), rabbit anti-PYGL (Proteintech; Cat#15851-1-AP), rabbit anti-NAGS (Abcam; Cat# ab65536), rabbit anti-CPS1 (Abcam; Cat# ab45956), rabbit anti-OTC (Novus Biologicals; Cat# NBP1-31582), mouse anti-ASS1 (Abcam; Cat# ab124465), rabbit anti-ASL (Abcam; Cat# ab201026), rabbit anti-ARG1 (Abcam; Cat# ab91279), mouse anti-β-actin (Novus Biologicals; Cat# NB600-501), mouse anti-GAPDH (Santa Cruz Biotechnology; Cat# sc-32233) Proteins of interest were detected with

horseradish peroxidase (HRP)-conjugated goat anti-rabbit IgG antibody (GE Healthcare). Peroxidase substrate was provided by ECL Western Blotting Substrate kit (Pierce). Densitometric analyses of the western blotting bands were performed using ImageJ Software.

Electron microscopy (EM). For EM analyses, liver specimens were fixed in 1% glutaraldehyde in 0.2M HEPES buffer. Small blocks of liver tissues were then post-fixed in OsO4 and uranyl acetate. After dehydration through a graded series of ethanol solutions and propylene oxide tissue samples were embedded in epoxy resin and polymerized at 60°C for 72 h. From each sample, thin sections were cut with a Leica EM UC7 ultramicrotome and images acquired by FEI Tecnai −12 (FEI, Einhoven, The Netherlands) EM equipped with Veletta CCD camera for digital image acquisition.

***Statistical analyses*.** Data were analysed using GraphPad Prism 5.0 software, San Diego, CA, USA. Comparisons of continuous variables between two or more experimental groups were performed using the two-tailed unpaired Student's *t* test or one-way ANOVA with Tukey's or Dunnett's post-hoc tests. Two-way ANOVA and Tukey's post-hoc tests were performed to compare two groups relative to two factors. Kaplan-Meier survival curves were compared with the Log-rank test. No statistical methods were used to predetermine the sample size. Data are expressed as means ± S.E.M. p values <0.05 were considered statistically significant.

ACKNOWLEDGMENTS

We thank Edoardo Nusco and Carmen Lanzara (TIGEM) for technical assistance in mouse studies. This work was supported by grants of Fondazione Telethon Italy (to N.B.-P.), MIUR (PRIN to N.B.-P.), NIHR Great Ormond Street Hospital Biomedical Research Centre (to J.B. and S.E.), MRC Clinician Scientist Fellowship MR/T008024/1 (J.B.) and Innovate UK (S.G., D.P.). The

views expressed are those of the author(s) and not necessarily those of the NHS, the NIHR or the Department of Health.

AUTHOR CONTRIBUTIONS

LRS performed study concept and design, acquisition of data, analysis, interpretation of data and wrote the manuscript; DPP performed studies in *Asl*$^{Neo/Neo}$ mice; GdS performed studies in *spf-ash* mice; AdA performed some Western blots; GB performed studies on *Becn1*^{F121A} mice; EP performed EM; DP analyzed ^{1}H-NMR data; PC performed ^{1}H-NMR; AM supervised ^{1}H-NMR studies; SG, MO, SE, SW participated to studies in *Asl*$^{Neo/Neo}$ mice; CS supervised studies on *Becn1*^{F121A} mice; AFM supervised studies in *spf-ash* mice; JB supervised studies in *Asl*$^{Neo/Neo}$ mice; NBP supervised the study, performed study concept and design, analysis and interpretation of data, and wrote the manuscript.

CONFLICT OF INTEREST

The authors declare no competing financial interests.

THE PAPER EXPLAINED

PROBLEM: Urea cycle disorders (UCD) have high morbidity and mortality. Novel and more effective therapies for UCD are needed.

RESULTS: Mice carrying a Beclin-1 activating mutation have increased ammonia detoxification. The cell penetrating autophagy inducing Tat-Beclin-1 (TB-1) peptide improved phenotypic and biochemical abnormalities of the two mouse models for the most common UCD, namely ornithine transcarbamylase (OTC) and argininosuccinate lyase (ASL) deficiencies.

IMPACT: Beclin-1-dependent activation therapy has potential for therapy of UCD.

REFERENCES

Allaire M, Rautou PE, Codogno P, Lotersztajn S (2019) Autophagy in liver diseases: Time for translation? *J Hepatol* 70**:** 985-998

Ashe KM, Taylor KM, Chu Q, Meyers E, Ellis A, Jingozyan V, Klinger K, Finn PF, Cooper CG, Chuang WL et al (2010) Inhibition of glycogen biosynthesis via mTORC1 suppression as an adjunct therapy for Pompe disease. *Mol Genet Metab* 100**:** 309-315

Ashley SN, Nordin JML, Buza EL, Greig JA, Wilson JM (2018) Adeno-associated viral gene therapy corrects a mouse model of argininosuccinic aciduria. *Mol Genet Metab* 125**:** 241-250

Badizadegan K, Perez-Atayde AR (1997) Focal glycogenosis of the liver in disorders of ureagenesis: its occurrence and diagnostic significance. *Hepatology* 26**:** 365-373

Bartolomeo R, Cinque L, De Leonibus C, Forrester A, Salzano AC, Monfregola J, De Gennaro E, Nusco E, Azario I, Lanzara C et al (2017) mTORC1 hyperactivation arrests bone growth in lysosomal storage disorders by suppressing autophagy. *J Clin Invest* 127**:** 3717-3729

Baruteau J, Diez-Fernandez C, Lerner S, Ranucci G, Gissen P, Dionisi-Vici C, Nagamani S, Erez A, Haberle J (2019a) Argininosuccinic aciduria: Recent pathophysiological insights and therapeutic prospects. *J Inherit Metab Dis* 42**:** 1147-1161

Baruteau J, Jameson E, Morris AA, Chakrapani A, Santra S, Vijay S, Kocadag H, Beesley CE, Grunewald S, Murphy E et al (2017) Expanding the phenotype in argininosuccinic aciduria: need for new therapies. *J Inherit Metab Dis* 40**:** 357-368

Baruteau J, Khalil Y, Grunewald S, Zancolli M, Chakrapani A, Cleary M, Davison J, Footitt E, Waddington SN, Gissen P et al (2019b) Urea Cycle Related Amino Acids Measured in Dried Bloodspots Enable Long-Term In Vivo Monitoring and Therapeutic Adjustment. *Metabolites* 9

Baruteau J, Perocheau DP, Hanley J, Lorvellec M, Rocha-Ferreira E, Karda R, Ng J, Suff N, Diaz JA, Rahim AA et al (2018) Argininosuccinic aciduria fosters neuronal nitrosative stress reversed by Asl gene transfer. *Nat Commun* 9**:** 3505

Bigot A, Tchan MC, Thoreau B, Blasco H, Maillot F (2017) Liver involvement in urea cycle disorders: a review of the literature. *J Inherit Metab Dis* 40**:** 757-769

Burrage LC, Madan S, Li X, Ali S, Mohammad M, Stroup BM, Jiang MM, Cela R, Bertin T, Jin Z et al (2020) Chronic liver disease and impaired hepatic glycogen metabolism in argininosuccinate lyase deficiency. *JCI Insight* 5

Chiang WC, Wei Y, Kuo YC, Wei S, Zhou A, Zou Z, Yehl J, Ranaghan MJ, Skepner A, Bittker JA et al (2018) High-Throughput Screens To Identify Autophagy Inducers That Function by Disrupting Beclin 1/Bcl-2 Binding. *ACS Chem Biol* 13**:** 2247-2260

Cinque L, Forrester A, Bartolomeo R, Svelto M, Venditti R, Montefusco S, Polishchuk E, Nusco E, Rossi A, Medina DL et al (2015) FGF signalling regulates bone growth through autophagy. *Nature* 528**:** 272-275

DeMars R, LeVan SL, Trend BL, Russell LB (1976) Abnormal ornithine carbamoyltransferase in mice having the sparse-fur mutation. *Proc Natl Acad Sci U S A* 73**:** 1693-1697

Enns GM, Berry SA, Berry GT, Rhead WJ, Brusilow SW, Hamosh A (2007) Survival after treatment with phenylacetate and benzoate for urea-cycle disorders. *N Engl J Med* 356**:** 2282-2292

Erez A, Nagamani SC, Shchelochkov OA, Premkumar MH, Campeau PM, Chen Y, Garg HK, Li L, Mian A, Bertin TK et al (2011) Requirement of argininosuccinate lyase for systemic nitric oxide production. *Nat Med* 17**:** 1619-1626

Farah BL, Landau DJ, Sinha RA, Brooks ED, Wu Y, Fung SYS, Tanaka T, Hirayama M, Bay BH, Koeberl DD et al (2016) Induction of autophagy improves hepatic lipid metabolism in glucose-6-phosphatase deficiency. *J Hepatol* 64**:** 370-379

Fernandez AF, Sebti S, Wei Y, Zou Z, Shi M, McMillan KL, He C, Ting T, Liu Y, Chiang WC et al (2018) Disruption of the beclin 1-BCL2 autophagy regulatory complex promotes longevity in mice. *Nature* 558**:** 136-140

Haberle J, Burlina A, Chakrapani A, Dixon M, Karall D, Lindner M, Mandel H, Martinelli D, Pintos-Morell G, Santer R et al (2019) Suggested guidelines for the diagnosis and management of urea cycle disorders: First revision. *J Inherit Metab Dis* 42**:** 1192-1230

Hazari Y, Bravo-San Pedro JM, Hetz C, Galluzzi L, Kroemer G (2020) Autophagy in hepatic adaptation to stress. *J Hepatol* 72**:** 183-196

He M, Ding Y, Chu C, Tang J, Xiao Q, Luo ZG (2016) Autophagy induction stabilizes microtubules and promotes axon regeneration after spinal cord injury. *Proc Natl Acad Sci U S A* 113**:** 11324-11329

Hill SM, Wrobel L, Rubinsztein DC (2019) Post-translational modifications of Beclin 1 provide multiple strategies for autophagy regulation. *Cell Death Differ* 26**:** 617-629

Hodges PE, Rosenberg LE (1989) The spfash mouse: a missense mutation in the ornithine transcarbamylase gene also causes aberrant mRNA splicing. *Proc Natl Acad Sci U S A* 86**:** 4142-4146

Karsli-Uzunbas G, Guo JY, Price S, Teng X, Laddha SV, Khor S, Kalaany NY, Jacks T, Chan CS, Rabinowitz JD et al (2014) Autophagy is required for glucose homeostasis and lung tumor maintenance. *Cancer Discov* 4**:** 914-927

Kaur J, Debnath J (2015) Autophagy at the crossroads of catabolism and anabolism. *Nat Rev Mol Cell Biol* 16**:** 461-472

Kho J, Tian X, Wong WT, Bertin T, Jiang MM, Chen S, Jin Z, Shchelochkov OA, Burrage LC, Reddy AK et al (2018) Argininosuccinate Lyase Deficiency Causes an Endothelial-Dependent Form of Hypertension. *Am J Hum Genet* 103**:** 276-287

Koo M, Lipshutz GS, Cederbaum SD, Lassman C (2017) Biopsy-proven Hepatocellular Carcinoma in a 53-year-old Woman With Arginase Deficiency. *Pediatr Dev Pathol* 20**:** 517-521

Kurtz CB, Millet YA, Puurunen MK, Perreault M, Charbonneau MR, Isabella VM, Kotula JW, Antipov E, Dagon Y, Denney WS et al (2019) An engineered E. coli Nissle improves hyperammonemia and survival in mice and shows dose-dependent exposure in healthy humans. *Sci Transl Med* 11

Li J, Kim SG, Blenis J (2014) Rapamycin: one drug, many effects. *Cell Metab* 19**:** 373-379

Liang C, Lee JS, Inn KS, Gack MU, Li Q, Roberts EA, Vergne I, Deretic V, Feng P, Akazawa C et al (2008) Beclin1-binding UVRAG targets the class C Vps complex to coordinate autophagosome maturation and endocytic trafficking. *Nat Cell Biol* 10**:** 776-787

Martina JA, Diab HI, Lishu L, Jeong AL, Patange S, Raben N, Puertollano R (2014) The nutrient-responsive transcription factor TFE3 promotes autophagy, lysosomal biogenesis, and clearance of cellular debris. *Sci Signal* 7**:** ra9

Mori T, Nagai K, Mori M, Nagao M, Imamura M, Iijima M, Kobayashi K (2002) Progressive liver fibrosis in late-onset argininosuccinate lyase deficiency. *Pediatr Dev Pathol* 5**:** 597-601

Moscioni D, Morizono H, McCarter RJ, Stern A, Cabrera-Luque J, Hoang A, Sanmiguel J, Wu D, Bell P, Gao GP et al (2006) Long-term correction of ammonia metabolism and prolonged survival in ornithine transcarbamylase-deficient mice following liver-directed treatment with adeno-associated viral vectors. *Mol Ther* 14**:** 25-33

Nagamani SC, Campeau PM, Shchelochkov OA, Premkumar MH, Guse K, Brunetti-Pierri N, Chen Y, Sun Q, Tang Y, Palmer D et al (2012) Nitric-oxide supplementation for treatment of long-term complications in argininosuccinic aciduria. *Am J Hum Genet* 90**:** 836-846

Peraro L, Zou Z, Makwana KM, Cummings AE, Ball HL, Yu H, Lin YS, Levine B, Kritzer JA (2017) Diversity-Oriented Stapling Yields Intrinsically Cell-Penetrant Inducers of Autophagy. *J Am Chem Soc* 139**:** 7792-7802

Pietrocola F, Pol J, Vacchelli E, Rao S, Enot DP, Baracco EE, Levesque S, Castoldi F, Jacquelot N, Yamazaki T et al (2016) Caloric Restriction Mimetics Enhance Anticancer Immunosurveillance. *Cancer Cell* 30**:** 147-160

Prats C, Graham TE, Shearer J (2018) The dynamic life of the glycogen granule. *J Biol Chem* 293**:** 7089-7098

Prieve MG, Harvie P, Monahan SD, Roy D, Li AG, Blevins TL, Paschal AE, Waldheim M, Bell EC, Galperin A et al (2018) Targeted mRNA Therapy for Ornithine Transcarbamylase Deficiency. *Mol Ther* 26**:** 801-813

Ranucci G, Rigoldi M, Cotugno G, Bernabei SM, Liguori A, Gasperini S, Goffredo BM, Martinelli D, Monti L, Francalanci P et al (2019) Chronic liver involvement in urea cycle disorders. *J Inherit Metab Dis* 42**:** 1118-1127

Rocchi A, Yamamoto S, Ting T, Fan Y, Sadleir K, Wang Y, Zhang W, Huang S, Levine B, Vassar R et al (2017) A Becn1 mutation mediates hyperactive autophagic sequestration of amyloid oligomers and improved cognition in Alzheimer's disease. *PLoS Genet* 13**:** e1006962

Shoji-Kawata S, Sumpter R, Leveno M, Campbell GR, Zou Z, Kinch L, Wilkins AD, Sun Q, Pallauf K, MacDuff D et al (2013) Identification of a candidate therapeutic autophagy-inducing peptide. *Nature* 494**:** 201-206

Song X, Zhu S, Chen P, Hou W, Wen Q, Liu J, Xie Y, Liu J, Klionsky DJ, Kroemer G et al (2018) AMPK-Mediated BECN1 Phosphorylation Promotes Ferroptosis by Directly Blocking System Xc(-) Activity. *Curr Biol* 28**:** 2388-2399 e2385

Soria LR, Ah Mew N, Brunetti-Pierri N (2019) Progress and challenges in development of new therapies for urea cycle disorders. *Hum Mol Genet* 28**:** R42-R48

Soria LR, Allegri G, Melck D, Pastore N, Annunziata P, Paris D, Polishchuk E, Nusco E, Thony B, Motta A et al (2018) Enhancement of hepatic autophagy increases ureagenesis and protects against hyperammonemia. *Proc Natl Acad Sci U S A* 115**:** 391-396

Soria LR, Brunetti-Pierri N (2018) Targeting autophagy for therapy of hyperammonemia. *Autophagy* 14**:** 1273-1275

Soria LR, Brunetti-Pierri N (2019) Ammonia and autophagy: An emerging relationship with implications for disorders with hyperammonemia. *J Inherit Metab Dis* 42**:** 1097-1104

Spampanato C, Feeney E, Li L, Cardone M, Lim JA, Annunziata F, Zare H, Polishchuk R, Puertollano R, Parenti G et al (2013) Transcription factor EB (TFEB) is a new therapeutic target for Pompe disease. *EMBO Mol Med* 5**:** 691-706

Sun RC, Dukhande VV, Zhou Z, Young LEA, Emanuelle S, Brainson CF, Gentry MS (2019) Nuclear Glycogenolysis Modulates Histone Acetylation in Human Non-Small Cell Lung Cancers. *Cell Metab* 30**:** 903-916 e907

Sun Y, Yao X, Zhang QJ, Zhu M, Liu ZP, Ci B, Xie Y, Carlson D, Rothermel BA, Sun Y et al (2018) Beclin-1-Dependent Autophagy Protects the Heart During Sepsis. *Circulation* 138**:** 2247-2262

Vega-Rubin-de-Celis S, Zou Z, Fernandez AF, Ci B, Kim M, Xiao G, Xie Y, Levine B (2018) Increased autophagy blocks HER2-mediated breast tumorigenesis. *Proc Natl Acad Sci U S A* 115**:** 4176-4181

Wang L, Bell P, Morizono H, He Z, Pumbo E, Yu H, White J, Batshaw ML, Wilson JM (2017) AAV gene therapy corrects OTC deficiency and prevents liver fibrosis in aged OTC-knock out heterozygous mice. *Mol Genet Metab* 120**:** 299-305

Wang L, Wang L, Zhu S, Zhang M, Dong Y, Wang FS (2019) A 6-Year-Old Child With Citrin Deficiency and Advanced Hepatocellular Carcinoma. *Pediatrics* 143

Wilson JM, Shchelochkov OA, Gallagher RC, Batshaw ML (2012) Hepatocellular carcinoma in a research subject with ornithine transcarbamylase deficiency. *Mol Genet Metab* 105**:** 263-265

Yamamoto S, Kuramoto K, Wang N, Situ X, Priyadarshini M, Zhang W, Cordoba-Chacon J, Layden BT, He C (2018) Autophagy Differentially Regulates Insulin Production and Insulin Sensitivity. *Cell* Rep 23**:** 3286-3299

Yang Y, Wang L, Bell P, McMenamin D, He Z, White J, Yu H, Xu C, Morizono H, Musunuru K et al (2016) A dual AAV system enables the Cas9-mediated correction of a metabolic liver disease in newborn mice. *Nat Biotechnol* 34**:** 334-338

Yaplito-Lee J, Chow CW, Boneh A (2013) Histopathological findings in livers of patients with urea cycle disorders. *Mol Genet Metab* 108**:** 161-165

Ye X, Robinson MB, Batshaw ML, Furth EE, Smith I, Wilson JM (1996) Prolonged metabolic correction in adult ornithine transcarbamylase-deficient mice with adenoviral vectors. *J Biol Chem* 271**:** 3639-3646

FIGURE LEGENDS

Fig. 1. Hyperactive Beclin-1 protects against hyperammonemia and activation of hepatic autophagy improves the phenotype of OTC-deficient mice. (A) Blood ammonia in 8-9-week-old C57BL/6J wild-type (WT) mice (n=8) and *Becn1*^{F121A} mice with constitutive activation of autophagy (n=8) at baseline and 30 min after i.p. injection of NH_4Cl (10 mmol/kg). **p<0.01 (Unpaired t-test). ns: not statistically significant difference. **(B)** Urinary orotic acid of 12-week-old *spf-ash* mice treated with TB-1 (15 mg/kg, i.p) or vehicle at various times as indicated by the arrows (n=5 mice/group). *p<0.05 (Two-way ANOVA). **(C-D)** Western blotting and densitometric quantifications of autophagy markers (LC3II: autophagosomes; p62 and NBR1: cargo receptors) in livers of *spf-ash* mice harvested after ten days of treatment with TB-1 or vehicle. β-actin was used as loading control. n=5 mice/group. **p<0.01, *p<0.05 (Unpaired t-test). **(E)** Survival curves of

spf-ash mice fed with a high protein diet (HPD) for ten days and treated with TB-1 alone or combined with scavenger drug and L-Arginine, or treated with scavenger drug and L-Arginine, or left untreated. WT control were included n=5/group. ***p<0.001 (Log-rank Mantel-Cox test). **(F)** Blood ammonia levels determined after 4 days under HPD (n=5 mice/group); ***p<0.001, **p<0.01, *p<0.05 (One-way ANOVA). Treatments in **E-F**: Scavenger (Na-benzoate 250 mg/kg/day, i.p.) and L-arginine (L-Arg, 250 mg/kg/day, i.p.); TB-1 (15 mg/kg every 2 days, i.p). WT mice were age-, gender- and strain (C3H)-matched.

Fig. 2. Enhancement of liver autophagy improves survival, increases ureagenesis, and corrects metabolic defects of ASL-deficient mice. (A) Survival curves of $Asl^{Neo/Neo}$ mice and age-matched wild-type (WT) controls treated with TB-1 (15 mg/kg, i.p., every 48 hours starting at day 10 of age) or vehicle. WT + Vehicle n=8; WT + TB-1 n=8; $Asl^{Neo/Neo}$ + Vehicle n=20; $Asl^{Neo/Neo}$ + TB-1 n=16. *p<0.05 (Log-rank Mantel-Cox test). **(B)** Isotopic enrichment of ^{15}N-labeled urea in blood, 20 min after i.p. injection of $^{15}NH_4Cl$ tracer (4 mmol/kg) in $Asl^{Neo/Neo}$ mice treated with TB-1 (n=15) or vehicle (n=9). *p<0.05 (Unpaired t-test). **(C)** Representative Western blotting bands of LC3, p62 and NBR1 in livers of $Asl^{Neo/Neo}$ mice treated with TB-1 or vehicle. GAPDH and β-actin were used as loading controls. **(D)** Densitometric quantifications. $Asl^{Neo/Neo}$ + Vehicle n=5; $Asl^{Neo/Neo}$ + TB-1 n=9. **p<0.01, *p<0.05 (Unpaired t-test). **(E)** Orthogonal Projection to Latent Structure-Discriminant Analysis (OPLS-DA) score plot obtained from high-resolution ^{1}H-NMR spectroscopy performed on livers of vehicle-treated $Asl^{Neo/Neo}$ mice (n=6), WT controls (n=4) and $Asl^{Neo/Neo}$ mice injected with TB-1 (n=6). A statistical model with R^2=0.78 (goodness of fit), Q^2=0.57 (power in prediction) and p=0.0056 was obtained. **(F)** Argininosuccinate content by ^{1}H-NMR analysis in livers of WT mice, vehicle-treated $Asl^{Neo/Neo}$ mice, and TB-1–treated $Asl^{Neo/Neo}$ mice (n≥4/group). **p<0.01 (One-way ANOVA). ns: not statistically significant difference.

Fig. 3. Enhancement of autophagy reduces hepatocellular injury and glycogen storage in ASL-deficient mice. (A) Hematoxylin and eosin (H&E, upper panels) and periodic acid Schiff (PAS, lower panels) staining of liver samples harvested from WT and *Asl*$^{Neo/Neo}$ mice treated with TB-1 or vehicle. Scale bars: 500 μm. **(B)** Computational analysis of PAS staining (n≥4 mice/group). **p<0.01, *p<0.05 (One-way ANOVA). **(C)** Quantification of hepatic glycogen in vehicle (n=6)- and TB-1-treated *Asl*$^{Neo/Neo}$ mice (n=12) compared to WT (n=5) controls. **p<0.01, *p<0.05 (One-way ANOVA). **(D)** Representative Western blotting bands and densitometric quantification of PYGL **(D)** in livers of WT and *Asl*$^{Neo/Neo}$ mice treated with either with TB-1 or vehicle (n=4 mice/group). *p<0.05 (One-way ANOVA). GAPDH was used as loading control. **(E)** Representative electron microscopy images of liver samples harvested from WT and *Asl*$^{Neo/Neo}$ mice treated with TB-1 or vehicle. Scale bar: 900 nm.

Fig. 4. TB-1 reduces intra-nuclear glycogen deposition in ASL-deficient mice. (A) Representative electron microscopy images of liver samples harvested from WT and *Asl*$^{Neo/Neo}$ mice treated with TB-1 or vehicle. False color on the images indicates glycogen within the nuclei. Scale bar: 1 μm. **(B)** Quantification of nuclei containing glycogen (approx. 180 nuclei were analyzed in total per condition, n=3 mice/group).

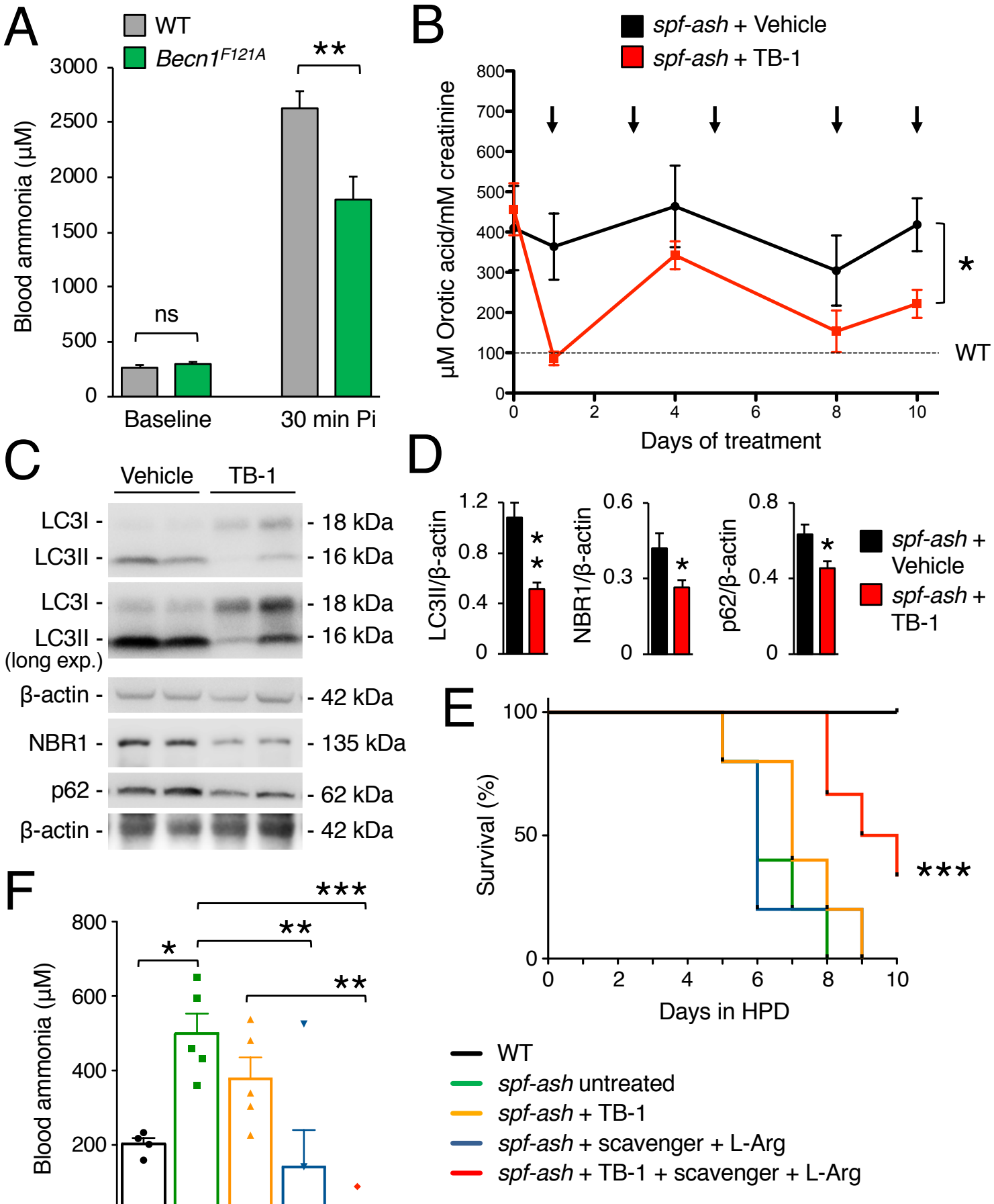
A
WT
Becn1F121A
Blood ammonia (μM)
3000
2500
2000
1500
1000
500
0
**
ns
Baseline
30 min Pi
B
spf-ash + Vehicle
spf-ash + TB-1
μM Orotic acid/mM creatinine
800
700
600
500
400
300
200
100
0
*
WT
0
2
4
6
8
10
Days of treatment
C
Vehicle
TB-1
LC3I -
LC3II -
- 18 kDa
- 16 kDa
LC3I -
LC3II -
(long exp.)
- 18 kDa
- 16 kDa
β-actin -
- 42 kDa
NBR1 -
- 135 kDa
p62 -
- 62 kDa
β-actin -
- 42 kDa
D
LC3II/β-actin
1.2
0.8
0.4
0
* *
NBR1/β-actin
0.6
0.3
0
*
p62/β-actin
0.8
0.4
0
*
spf-ash + Vehicle
spf-ash + TB-1
E
Survival (%)
100
50
0
0
2
4
6
8
10
Days in HPD
***
WT
spf-ash untreated
spf-ash + TB-1
spf-ash + scavenger + L-Arg
spf-ash + TB-1 + scavenger + L-Arg
F
Blood ammonia (μM)
800
600
400
200
0
*
**
**
***

Fig. 1

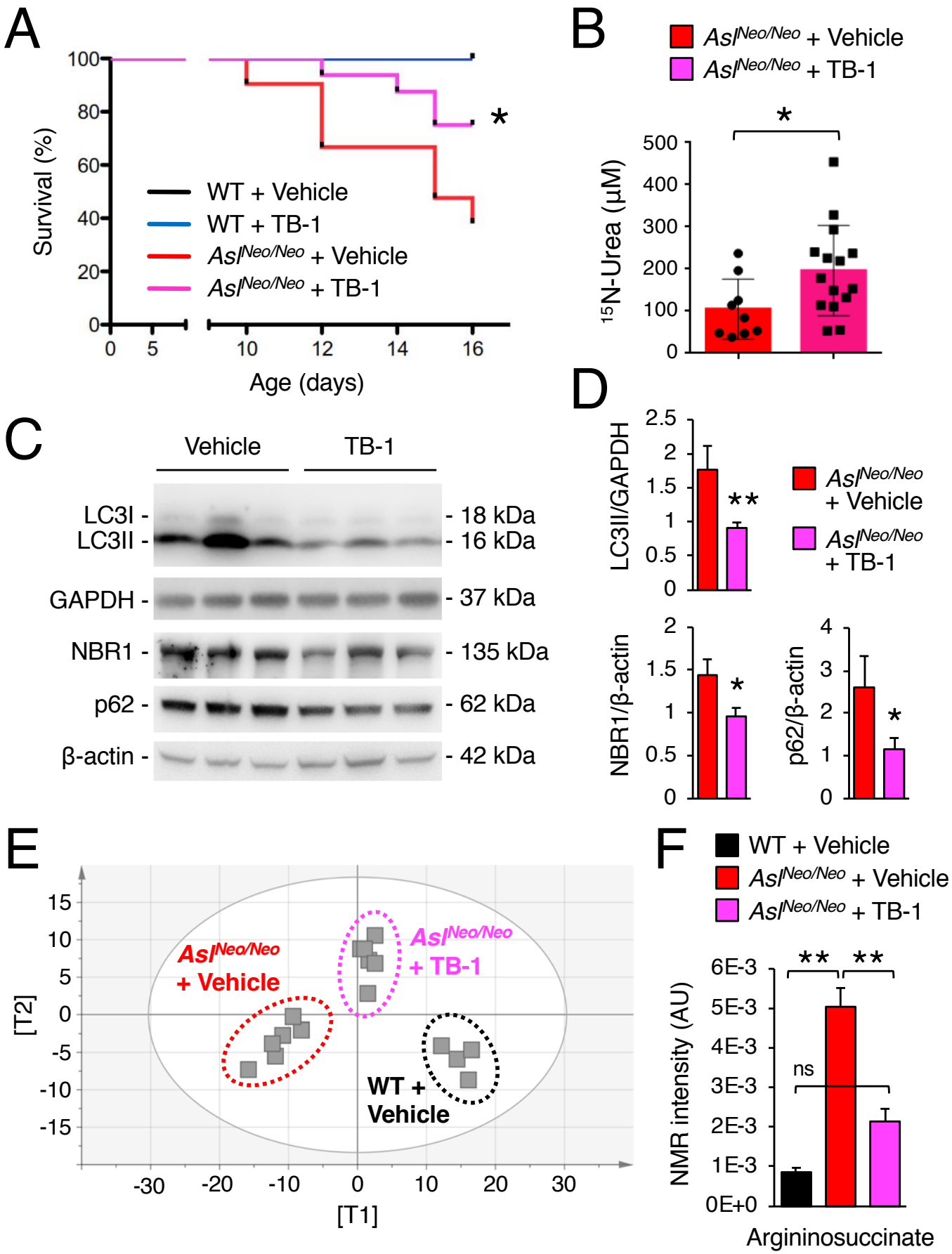
A
Survival (%)
100
80
60
40
20
0
0 5 10 12 14 16
Age (days)
WT + Vehicle
WT + TB-1
Asl Neo/Neo + Vehicle
Asl Neo/Neo + TB-1
*
B
Asl Neo/Neo + Vehicle
Asl Neo/Neo + TB-1
*
15N-Urea (μM)
500
400
300
200
100
0
C
Vehicle
TB-1
LC3I -
LC3II -
- 18 kDa
- 16 kDa
GAPDH - 37 kDa
NBR1 - 135 kDa
p62 - 62 kDa
β-actin - 42 kDa
D
LC3II/GAPDH
2.5
2
1.5
1
0.5
0
**
Asl Neo/Neo + Vehicle
Asl Neo/Neo + TB-1
NBR1/β-actin
2
1.5
1
0.5
0
*
p62/β-actin
4
3
2
1
0
*
E
15
10
5
0
-5
-10
-15
[T2]
-30 -20 -10 0 10 20 30
[T1]
Asl Neo/Neo + Vehicle
Asl Neo/Neo + TB-1
WT + Vehicle
F
WT + Vehicle
Asl Neo/Neo + Vehicle
Asl Neo/Neo + TB-1
NMR intensity (AU)
6E-3
5E-3
4E-3
3E-3
2E-3
1E-3
0E+0
** **
ns
Argininosuccinate

Fig. 2

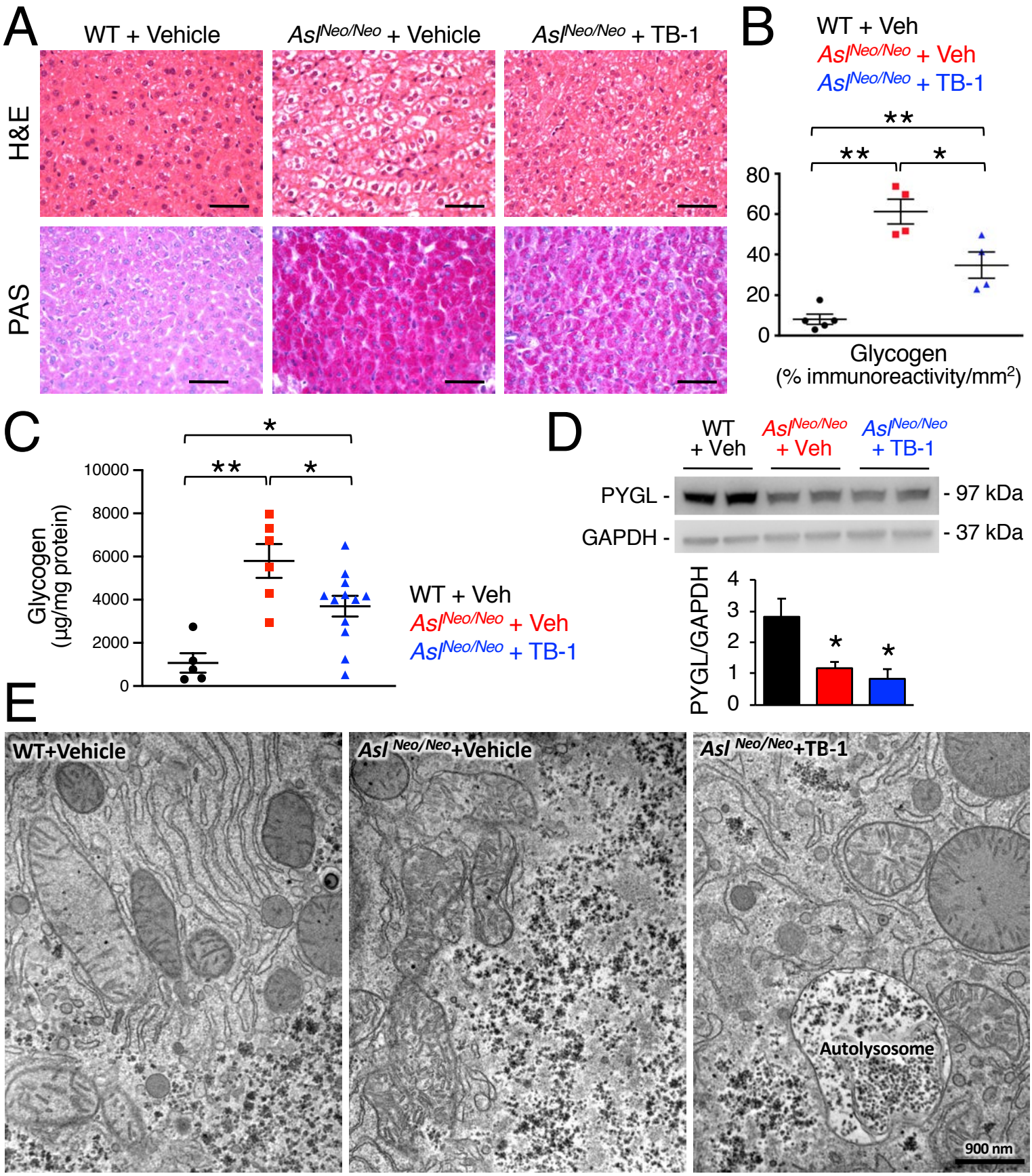
A
WT + Vehicle
Asl Neo/Neo + Vehicle
Asl Neo/Neo + TB-1
H&E
PAS
B
WT + Veh
Asl Neo/Neo + Veh
Asl Neo/Neo + TB-1
**
**
*
80
60
40
20
0
Glycogen
(% immunoreactivity/mm2)
C
*
**
*
10000
8000
6000
4000
2000
0
Glycogen
(µg/mg protein)
WT + Veh
Asl Neo/Neo + Veh
Asl Neo/Neo + TB-1
D
WT
+ Veh
Asl Neo/Neo
+ Veh
Asl Neo/Neo
+ TB-1
PYGL -
- 97 kDa
GAPDH -
- 37 kDa
PYGL/GAPDH
4
3
2
1
0
*
*
E
WT+Vehicle
Asl Neo/Neo+Vehicle
Asl Neo/Neo+TB-1
Autolysosome
900 nm

Fig. 3

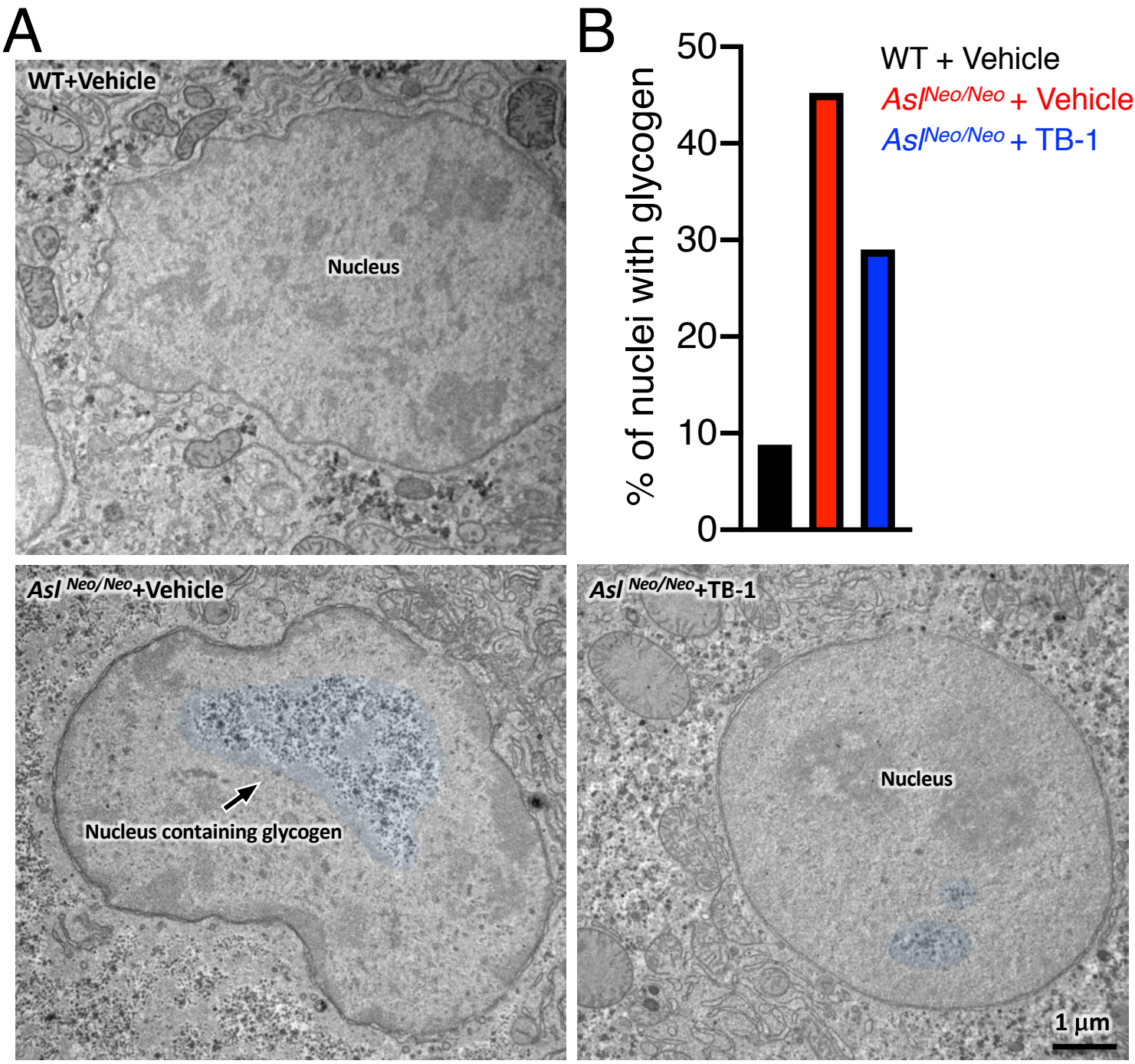
A
WT+Vehicle
Nucleus
B
% of nuclei with glycogen
50
40
30
20
10
0
WT + Vehicle
Asl Neo/Neo + Vehicle
Asl Neo/Neo + TB-1
Asl Neo/Neo+Vehicle
Nucleus containing glycogen
Asl Neo/Neo+TB-1
Nucleus
1 µm

Fig. 4